Int. J. Electrochem. Sci., 16 **(2021)** Article Number: 211148, doi: 10.20964/2021.11.52

International Journal of
ELECTROCHEMICAL
SCIENCE
www.electrochemsci.org

Superior electrochemical performances of $LiTi_2(PO_4)_3$/C composite anode for aqueous lithium-ion battery

Xiaowei Wang

Henan Institute of Metrology, Zhengzhou 450000, China
E-mail: a292799736@sohu.com

Received: 2 July 2021 / *Accepted:* 22 August 2021 / *Published:* 10 October 2021

Aqueous rechargeable lithium battery has attracted widespread attention due to their environmental friendliness, long service life, and high safety. $LiTi_2(PO_4)_3$ anode exhibits a promising prospect considering its high structural stability and enhanced energy density. In this work, $LiTi_2(PO_4)_3$/carbon composite has been synthesized by using folic acid as a superior carbon source. The high-quality carbon not only protects the electrode from corrosion but also increases its electrical conductivity. A series of composites with different carbon content were prepared, and the effectiveness of the as-synthesized materials was further carried out systematically. Results show that the composite with a carbon content of 7.1% (LTP-F-2) exhibits the optimal electrochemical performance and a good stabilization mechanism. The discharge capacities of LTP-F-2 at 0.5, 4, and 15 C are 109, 108, and 95 mAh g^{-1}, respectively, which are 33, 76, and 82 mAh g^{-1} higher than those of pristine $LiTi_2(PO_4)_3$ (LTP). LTP-F-2 delivers the discharge capacity of 102 mAh g^{-1} at 0.5 C after 100 cycles and 83 mAh g^{-1} at 6 C after 1000 cycles. The capacity retention of LTP-F-2 at 6 C is 89.3% without significant corrosion on the electrode surface. Taking together, the result above reveals that folic acid-derived $LiTi_2(PO_4)_3$/carbon composite is an excellent alternative anode material in aqueous rechargeable lithium batteries.

Keywords: $LiTi_2(PO_4)_3$/C composite,queous lithium-ion battery, anode

1. INTRODUCTION

Nowadays, energy crises and environmental issues are two huge challenges with rapid economic development [1-3]. The combustion of traditional energy sources such as coal and petroleum led to the generation of large amounts of harmful gas and dust, which seriously pollute atmospheric environments, increase the PM 2.5 value, and further endanger human health [4]. Moreover, traditional energy reserves are non-renewable and thus limited. Accordingly, new energy sources, such as wind, solar, and tidal energy, have been developed [5, 6]. Although these energy sources have reduced environmental pollution obviously, they are greatly affected by natural causes, such as weather, season, and region. These energy sources are intermittent and unstable, further limiting their

effectiveness and reasonable use [7-9]. Therefore, in order to alleviate energy crisis and environmental pressure, there appears imminent including the rational development and usage of large-scale clean energy conversion and storage systems. Electrochemical energy storage utilizes reversible chemical reactions to convert electrical and chemical energy, and further accomplish the charging and discharging process. A lithium-ion cell is a battery that can be charged and discharged repeatedly. It has the characteristics of good cycling performance, large energy efficiency, and low process cost [10, 11], and is thus a promising energy storage system. In addition to its wide use in portable electronic devices such as laptop computers, and mobile phones, lithium battery has also been widely used in large devices including electric cars and electric motorcycles [12].

In general, traditional lithium-ion batteries use organic electrolytes. Unfortunately, most organics have toxicity and flammability, which cause explosion and combustion, and show potential hazards [13]. After the repeated charge and discharge process, the electrochemical stability may be deteriorated. Currently, the safety and electrochemical performance are required to be addressed. It is a high likelihood that aqueous rechargeable lithium batteries could be utilized to solve the problems. The security can be improved by using inorganic electrolytes such as Li_2SO_4 and $LiNO_3$ [14]. Additionally, aqueous rechargeable lithium battery also exhibits the advantages of simple assembly conditions, low cost, high conductivity, excellent rate performance, and low self-discharge [15]. In the 1990s, Dahn' group [16] first used a green inorganic slightly alkaline $LiNO_3$ electrolyte to construct a VO_2//$LiMn_2O_4$ battery. The operating voltage of the battery was determined to be about 1.5 V and the energy density reached 75 Wh kg^{-1}. The cycle performance was not satisfactory, but the first attempt proved that the use of inorganic electrolytes to build lithium-ion batteries was feasible and had the potential for development. Since the advent of aqueous rechargeable lithium battery, various aqueous rechargeable lithium battery systems have been reported, such as LiV_3O_8//$LiMn_2O_4$ [17], $NaTi_2(PO_4)_3$//$LiMn_2O_4$ [18], and NaV_6O_{15}//$LiMn_2O_4$ [19]. Precious studies also show that spinel-type $LiMn_2O_4$ cathode materials usually exhibit higher stability in aqueous electrolytes [20]. Joachim' group [21] assembled the activated carbon//0.5 mol L^{-1} Li_2SO_4 solution//$LiMn_2O_4$ battery system. The capacity retention of porous $LiMn_2O_4$ reached 93% after 10000 cycles at 9 C, which demonstrates it could be used for a long time without maintenance. However, due to anode material decomposition in the electrolyte after multiple cycles, the instability of anodes is considered as the main reason for the poor cycle performance of batteries [21]. Therefore, it is very significant to develop anode materials with proper lithium intercalation potential and better stability.

NASICON-type $LiTi_2(PO_4)_3$ possesses a rhombohedral crystal type, and the space group belongs to R3c [22]. Its main structure is formed by TiO_6 octahedron and PO_4 tetrahedron with shared oxygen atoms, and lithium is interspersed in interstitial sites along the c-axis direction (M1 and M2 site) [23]. The good thermal stability can be attributable to a strong P-O covalent bond. Open space channel provides wide pathways for the intercalation and deintercalation of lithium ions [24]. In addition, $LiTi_2(PO_4)_3$-based electrodes can be facilely prepared, which implies its high potential as an anode in an aqueous rechargeable lithium battery. However, $LiTi_2(PO_4)_3$ has poor electrical conductivity and structural stability in an aqueous solution [25]. As known, carbon coating can not only significantly improve the electrical conductivity of composites, but also protect the internal materials from electrolyte corrosion, resulting in the superior performances [26, 27]. For example,

Wang' group [28] prepared $LiTi_2(PO_4)_3$ nanoporous microplate coated with a 10 mm thick carbon layer, which shows a high discharge specific capacity and good stability resulting from the carbon layer.

In the work, a $LiTi_2(PO_4)_3$/carbon composite anode was synthesized by using folic acid as a carbon source. Folic acid is composed of teridine, p-aminobenzoic acid, and glutamic acid, containing a large amount of nitrogen and oxygen elements. The defects easily form on the surface of carbon during the carbonization process, which is conducive to the intercalation and deintercalation of lithium ions [29]. As a consequence, composites with high-quality carbon and $LiTi_2(PO_4)_3$ was synthesized. Of note, the carbon introduced from folic acid is utilized to protect the electrode and enhance the electrical conductivity, further facilitating the rate and cycling performances of the $LiTi_2(PO_4)_3$-based electrode. The microscopic surface structure and electrochemical performance of the as-synthesized composites are further studied systematically.

3. RESULTS AND DISCUSSION

2.1. Synthesis

Fig. 1 shows X-ray diffraction spectra of prepared LTP and LTP-F. According to Fig. 1, the spectra of all composites are similar in shape and characteristic peaks. It indicates that the materials used are relatively pure, and NASICON-type rhombohedal $LiTi_2(PO_4)_3$ crystal systems (JCPDS #035-0754) and belong to the R3c space group. However, LTP-F-3 was found to have a group of weak and broad miscellaneous peaks around $2\theta=35°$, which corresponds to $LiTi_2(PO_4)_3$ (JCPDS #024-0660) with other crystal forms. However, there is a very small amount of products and they exerted little effect on the main structure of electrodes. Taking together, results of XRD analysis show that neither the ball milling method nor the addition of folic acid as a carbon source has a significant effect on electrode structure.

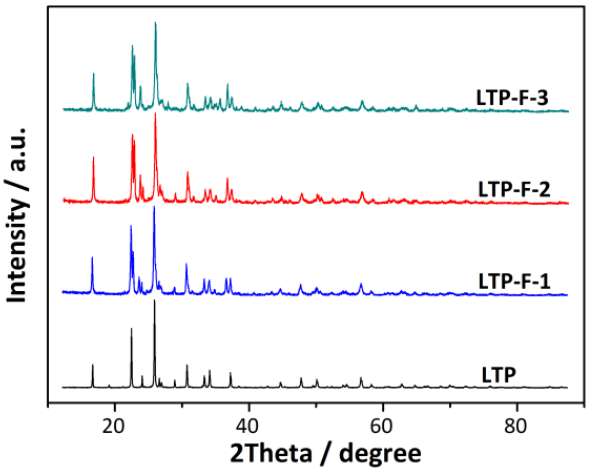

Figure 1. XRD patterns of all composites in the range of 10-90 degree.

Fig. 2 depicts SEM images of LTP and LTP-F-2 at low and high magnifications. There is no difference in the surface morphology of the two materials. The primary particles are mainly nano-sized, and the secondary ones are micro-sized due to the agglomeration phenomenon in the calcination process. Obviously, the smaller the particle size is, the faster the lithium-ion migration is.

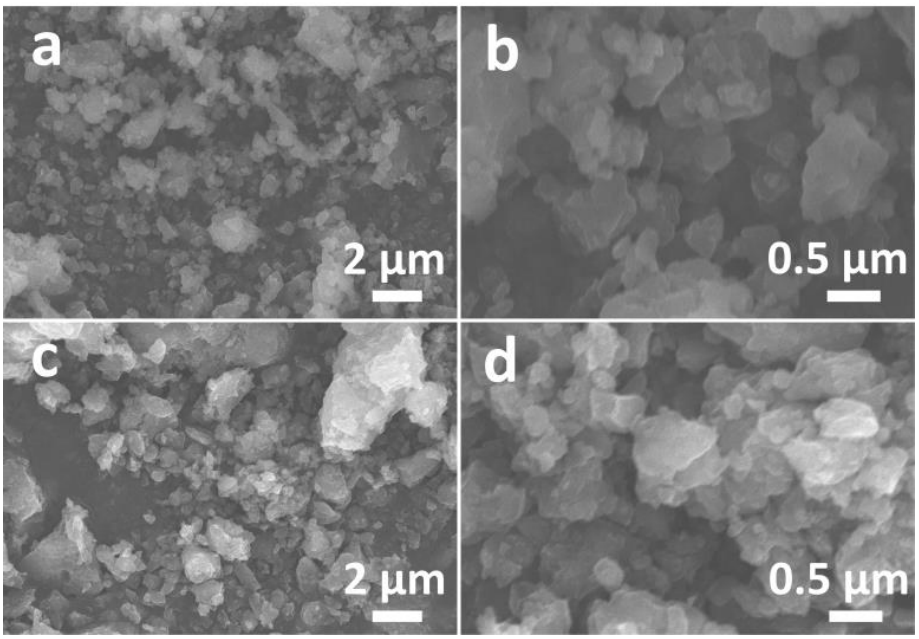

Figure 2. SEM images of LTP (a, b) and LTP-F-2 (c, d) at different amplifications.

Fig. 3 presents the result of TGA where the carbon content of composites was determined. The first weight loss platform with the weight loss was measured as about 1% in a range of 100~150 °C, which is ascribed to the volatilization of adsorbed water. As with increases in the temperature, there appear the second weight loss platforms except for the LTP sample. The second large platform of other samples at 400~600 °C is ascribed to the carbon combustion [25]. Compared with that of LTP, the carbon content of LTP-F-1, LTP-F-2, and LTP-F-3 is determined to be 4.7%, 7.1%, and 9.9%, separately. Accordingly, suitable carbon content facilitates the electrochemical performance of electrodes.

The contact angle of LTP and LTP-F-2 obtained from the water contact angle analysis is shown in Fig. 4. LTP exhibited a contact angle of 64.6°; comparatively, the contact angle of LTP-F-2 was decreased to 37.7°. Thus LTP-F-2 should be more hydrophilic in comparison with LTP, which is probably due to that some nitrogen and oxygen elements have been doped on the surface of the carbon. The doping of heteroatom and a raise in hydrophilicity could facilitate the migration of lithium ions on the electrode surface [30]. Moreover, doping heteroatom led to the generation of surface defects, and the improvement of the intercalation/decalation ability of lithium ions.

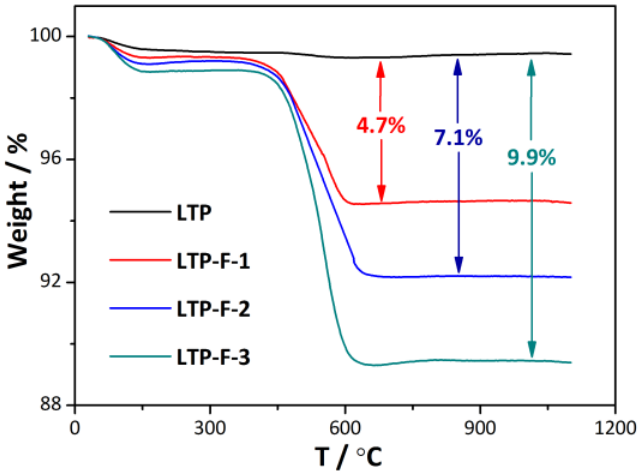

Figure 3. TGA curves of all composites from 25 °C to 1100 °C with the rate of 10 °C min^{-1}.

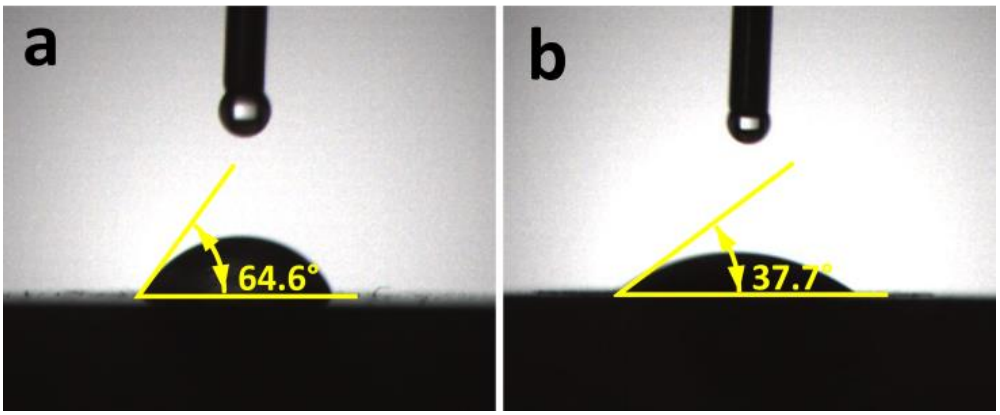

Figure 4. Contact angle of water droplet on LTP (a) and LTP-F-2 (b) coated graphite plates.

LTP and LTP-F materials were assembled into a cell and cycled for 5 cycles at various current densities for the rate test. According to Fig. 5a, the discharge capacity of LTP-F material is significantly higher than that of LTP, especially at high rates. However, excessive carbon can hinder the intercalation/deintercalation process of lithium ions, resulting in inferior electrochemical performances. Moreover, the presence of a minor amount of impurity crystal also resulted in the declined LTP-F rate performance. LTP-F-2 shows the best amongst all materials. The discharge capacities of LTP-F-2 at 0.5, 4, and 15 C are determined to be 109, 108, and 95 mAh g^{-1}, respectively, which are 33, 76, 82 mAh g^{-1} higher than those of LTP. The results are primarily because the high-quality carbon from folic acid facilitates the conductivity and the moving speed of electrons. The discharge capacity of the first few turns is unstable, probably due to the electrode activation process. In general, there is a uniform change trend of all materials. Improving the current led to an increase in the electrochemical polarization, and a gradual decrease in the discharge capacity. However, the declined rate of the LTP-F sample is significantly lower than that of blank LTP.

Previous studies on performance comparison of $LiTi_2(PO_4)_3$-based composites as the anode of ARLB are presented in Table 1. $LiTi_2(PO_4)_3$-based composite using folic acid as the carbon source

exhibited excellent rate performances compared with other $LiTi_2(PO_4)_3$-based composites. This is probably attributed to the special carbon source and thus more defects on carbon, further promoting intercalation/deintercalation ability [29]. Fig. 5b and Fig. 5c further show charge-discharge curves of LTP and LTP-F-2 at different rates. Both LTP and LTP-F-2 have obvious charging and discharging platform near 1.5 V. The platform of LTP-F-2 is wider and more stable than LTP at a high rate. So LTP-F-2 shows good stability and electrochemical performance. A narrow platform of around 1.1 V was observed for LTP-F-2, while not achieved for LTP. The phenomenon corresponds to the CV curve of LTP. As shown in Fig. 5d, the mean discharge voltage of LTP and LTP-F-2 are compared at different rates. The mean discharge voltage of LTP-F-2 is always higher than those of LTP, which is more obvious at high rates. The mean discharge voltage of LTP-F-2 and LTP is 1.46 and 1.14 V at 12 C, respectively. The larger mean discharge voltage facilitates the energy density in cells.

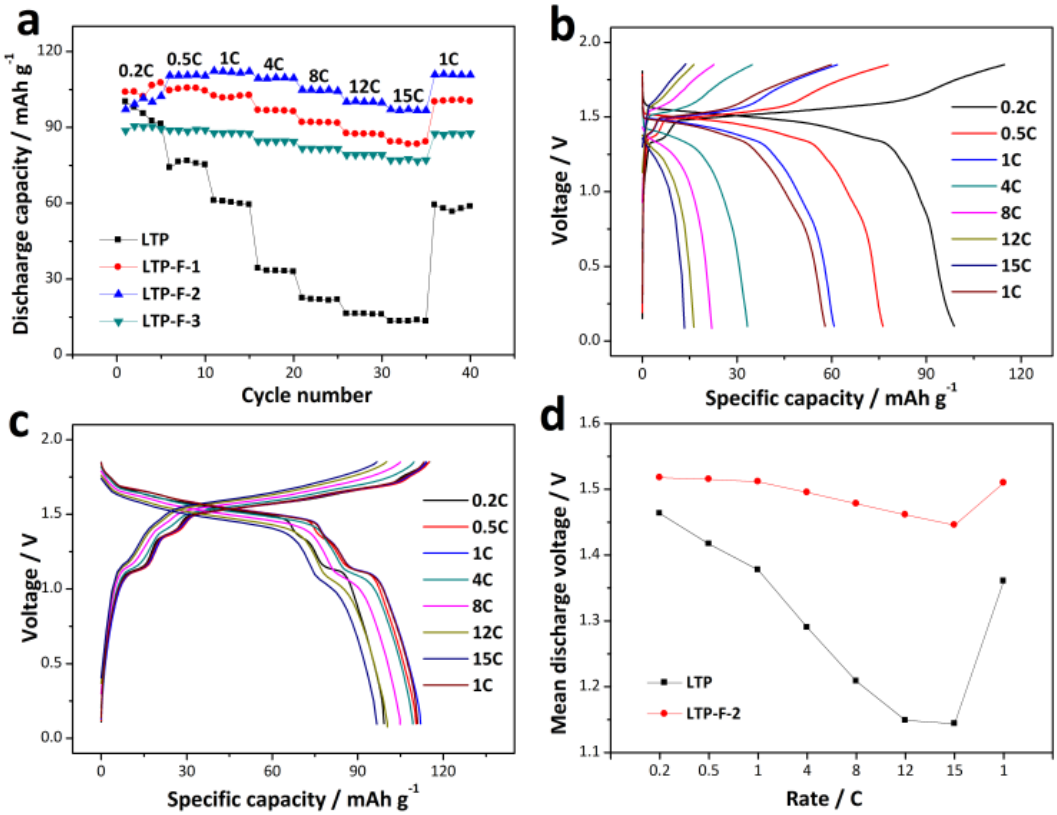

Figure 5. Rate performances of all samples at various rates (a), corresponding charge and discharge curves of LTP (b) and LTP-F-2 (c) composites, corresponding mean discharge voltages of LTP and LTP-F-2 composites at various rates (d).

Fig. 6 shows the CV results of cells assembled with different materials. The appearance of redox peaks corresponds to the intercalation/intercalation process of lithium ions. All materials except for LTP, present a pair of redox peaks around 1.1 V without significant difference. Comparatively, all samples show a large pair of redox peaks around 1.5 V with a enhanced order of peak current density: LTP < LTP-F-3 < LTP-F-1 < LTP-F-2. Thereby, LTP-F-2 exhibits the largest peak current density amongst all the tested samples, which is consistent with the results of their rate performance. This

indicates that the high-quality carbon effectively protects the electrode structure, and thus reduces the electrolyte corrosion for electrodes [36]. Moreover, the introduced carbon improves electrical conductivity. Additionally, the peak potential differences of LTP and LTP-F-2 are measured to be 0.13 V and 0.07 V, respectively, at around 1.5 V. The peak potential difference of LTP-F-2 is much smaller, indicating a decrease in the polarization degree of the cell and an increase in the electrochemical reversibility.

Table 1 Performance comparison of $LiTi_2(PO_4)_3$-based composites as anode of ARLB reported by literature.

No.	Anodes	Methods and sources	Discharge capacity/Rate	Refer.
1	$LiTi_2(PO_4)_3$/C nanoparticle	Sol-gel + chemical vapor deposition, toluene as C source	103 mAh g^{-1}/10 C	[31]
2	$LiTi_2(PO_4)_3$/C microplate	Solvothermal method, ethylenediamine as C source	76 mAh g^{-1}/20 C	[28]
3	$LiTi_2(PO_4)_3$/C-N nanoparticle	Sol-gel method, phenolic resin and urea as C and N sources	74.2 mAh g^{-1}/20 C	[32]
4	$LiTi_2(PO_4)_3$/C-N nanoparticle	One-pot carbonization + sol–gel method, pitch and $C_2H_8N_2$ as C and N sources	64 mAh g^{-1}/20 C	[33]
5	$LiTi_2(PO_4)_3$/C-N nanoparticle	Sol-gel method, PAN as C and N sources	79.1 mAh g^{-1}/20 C	[29]
6	$LiTi_2(PO_4)_3$/C nanoparticle	Sol-gel method, oxalic acid and glucose as C sources	54.2 mAh g^{-1}/20 C	[20]
7	$LiTi_2(PO_4)_3$/C nanoparticle	One-pot sintering process, pitch as C source	89 mAh g^{-1}/10 C	[34]
8	$LiTi_2(PO_4)_3$/C nanoparticle	Co-precipitation + anneal treatment, phytic acid as C source	92.5 mAh g^{-1}/10 C	[35]
9	$LiTi_2(PO_4)_3$/C nanoparticle	Solid state reaction, folic acid as C source	95 mAh g^{-1}/15 C	This work

To further explore the improvement effect of carbon from folic acid, LTP and LTP-F-2 were assembled into cells for EIS analysis, and the results are shown in Fig. 7. The curve consists of a semicircle in the high-frequency region and a straight line in the low-frequency region. As known, the straight-line slope represents Warburg resistance of lithium-ion diffusion, and the size of semicircle diameter represents charge transfer resistance [37]. The charge transfer resistance of LTP-F-2 (10 Ω) is significantly lower than that of LTP (35 Ω), indicating the faster migration of lithium ions and electrons for LTP-F-2. Moreover, the intercept on the Z' axis indicates the ohmic resistance of the

system. The ohmic resistances of LTP-F-2 are 0.7 Ω, much smaller than that of LTP (2.8 Ω). The improved electrical conductivity of the material is attributable to the high-quality carbon, enhancing its rate performance.

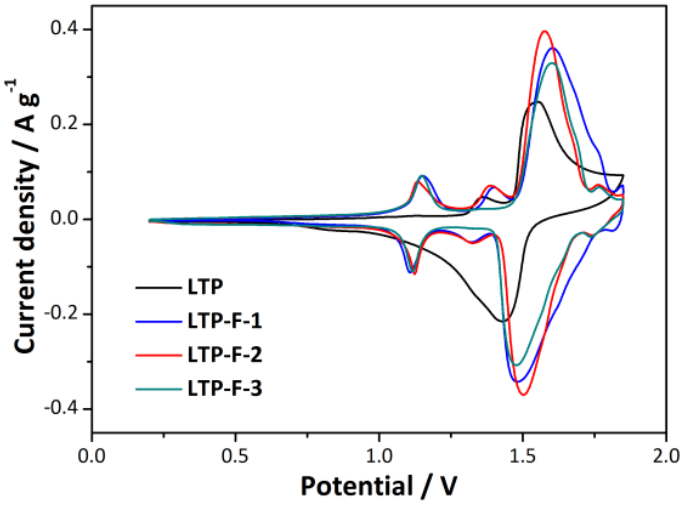

Figure 6. CV curves of all samples in the range of 0.2-1.8 V at a scan rate of 0.4 mV s^{-1}.

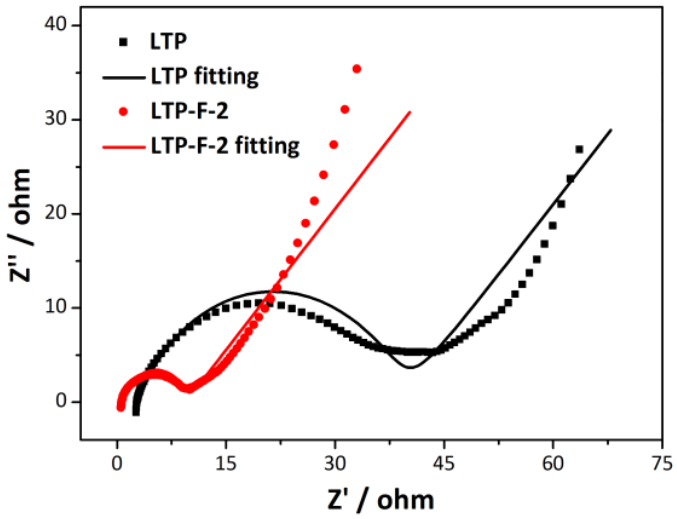

Figure 7. EIS results of LTP and LTP-F-2 composites in the range of 10^5 to 10^{-2} Hz with the amplitude of 5 mV.

The cycle performance was tested at two current densities. Discharge capacity and current efficiency comparison are shown in Fig. 8. At both current densities, the discharge capacity of LTP-F-2 is significantly improved compared to that of LTP. After 100 cycles at 0.5 C, the capacity of LTP-F-2 remains at 102 mAh g^{-1}, while LTP keeps at only 60 mAh g^{-1}. After 1000 cycles, the discharge

capacity of LTP-F-2 is relatively stable, and that of LTP has a downward trend. The capacity retention of LTP are 64.3% and 44.9% at 0.5 C and 6 C, separately; and those of LTP-F-2 are 96.1% and 89.3%, respectively. As presented in Fig. 8, the capacity retention of LTP-F-2 has been largely improved compared with that of pristine LTP, indicating that cycle performance becomes more stable probably due to the protection by a high-quality carbon. The current efficiency is above 100% for LTP and LTP-F-2, implying that the cell self-discharge is significantly low, and the small energy loss is a prominent feature of an aqueous rechargeable lithium battery.

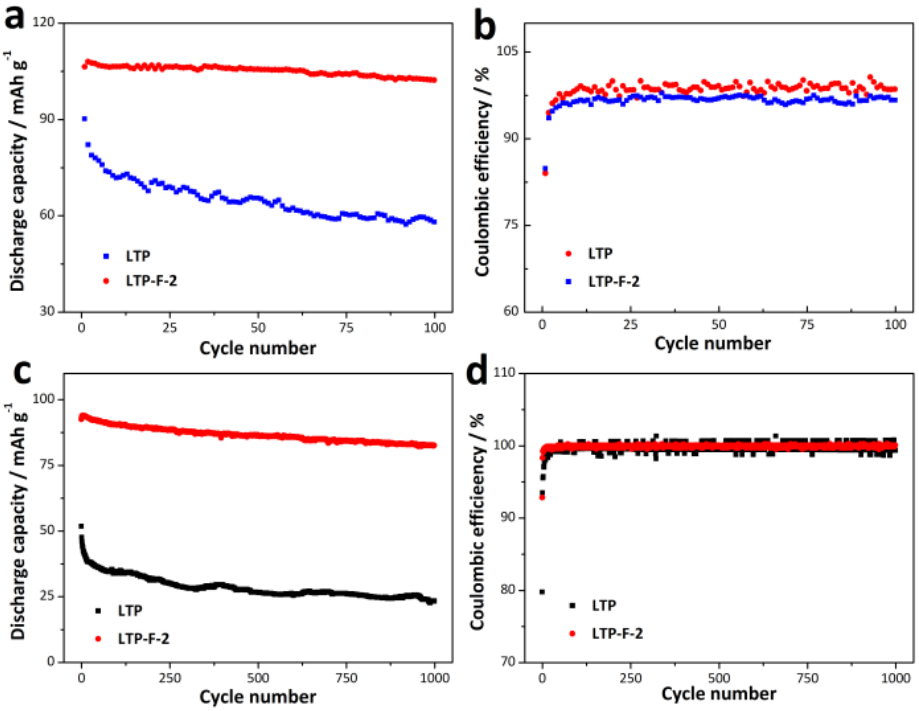

Figure 8. Cycling performance of LTP and LTP-F-2 at 0.5 C (a) and 6 C (c), corresponding coulombic efficiency of LTP and LTP-F-2 at 0.5 C (b) and 6 C (d).

Fig. 9 shows charge-discharge curves for LTP and LTP-F-2 at 6 C after 100, 200, 400, 700, and 1000 cycles. LTP-F-2 has narrow charging and discharging platform at 1.1 V, and a wide platform at 1.5 V. However, LTP shows a wide charging and discharging platform around 1.5 V. Additionally, the discharge voltage of LTP-F-2 is higher, and the shape of the platform maintains well after 1000 cycles, which fully indicates that the cell assembled by LTP-F-2 shows the optimal cycling performances and their stability.

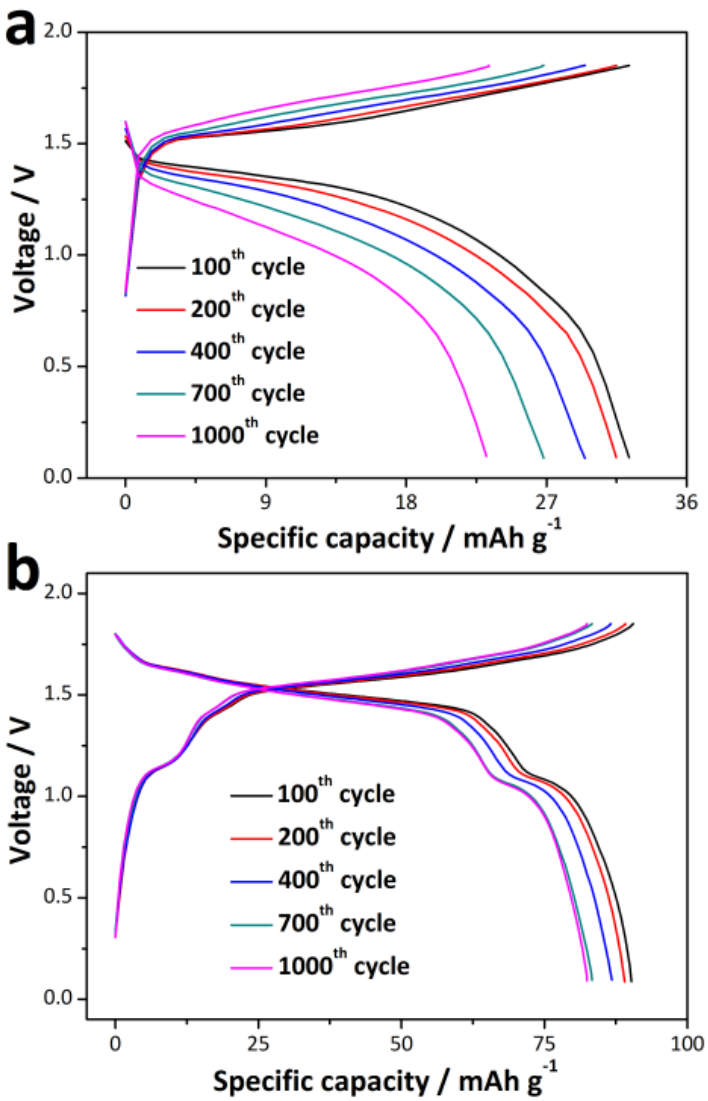

Figure 9. Charge and discharge curves of the cells using LTP (a) and LTP-F-2 (b) composites at a rate of 6 C after different cycles.

To further investigate the influence of high-quality carbon on the structural stability of electrodes, the LTP-F-2 electrodes after 100, 500, and 1000 cycles at 6 C were subjected to SEM analysis. As shown in Fig. 10, the surface of the LTP-F-2 electrode is relatively smooth after several cycles. There is no obvious decomposition and etching on the electrode surface after 1000 cycles. In other words, LTP-F-2 can keep stable morphology during the long-term charging and discharging process. As a consequence, the cell can obtain palmary cycling performance, which is in accordance with the excellent cycling performances in Fig. 8.

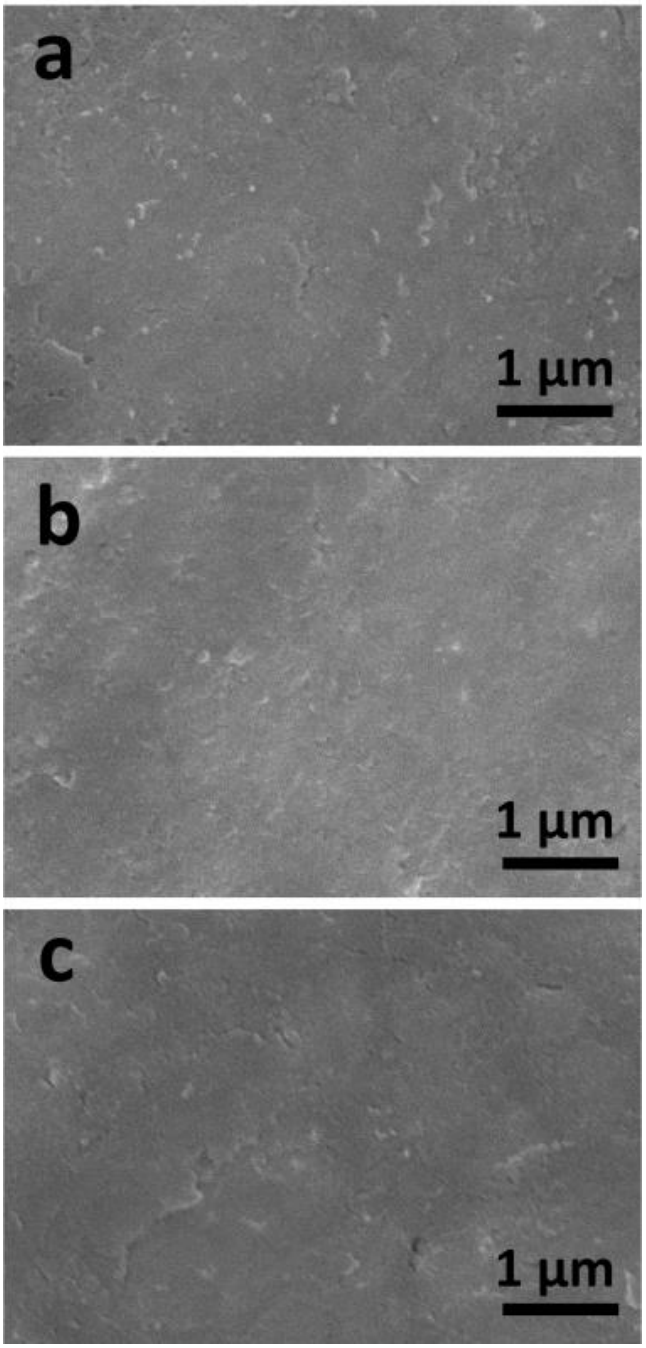

Figure 10. SEM images of LTP-F-2 electrode after 100 (a), 500 (b), and 1000 (c) cycles at a rate of 6 C.

Based on the stability of the material structure, electrochemical performance tests of LTP-F-2 after different cycles were also performed accordingly. Fig. 11a shows the CV curve comparison of the cell at 6 C after different cycles. The redox peaks around 1.1 V barely change. The peak current densities around 1.5 V slightly decrease, but the peak shape is still very sharp. There is no significant increase in the peak potential difference, indicating that the good stability and reversibility of batteries after 1000 cycles. Fig. 11b shows the EIS comparison of LTP-F-2 at 6 C after different cycles. An unobvious change in the overall shape of the curve was observed, and meanwhile, a slight increase in

the ohmic resistance and the charge transfer resistance was obtained. It indicates that the good stability mechanism of LTP-F-2. This may be attributed to the improved electrical conductivity resulting from high-quality carbon, and the reduced electrochemical polarization. Moreover, the proper carbon content can prevent direct contact between electrolyte and electrode, and protect the electrode from corrosion.

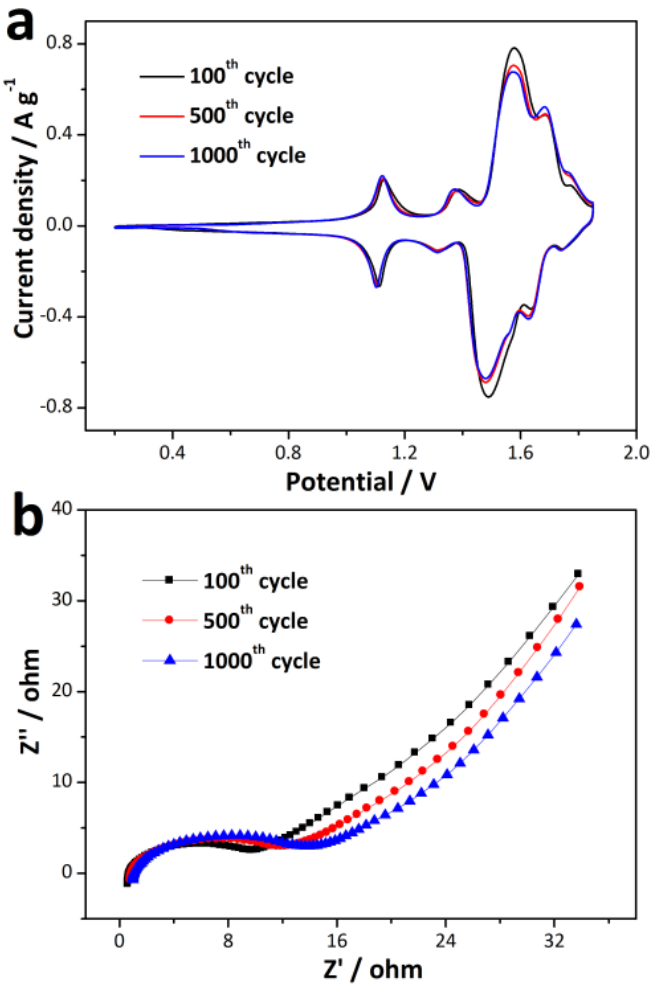

Figure 11. CV curves (a) at a scan rate of 0.4 mV s^{-1} and EIS results (b) in the range of 10^5 to 10^{-2} Hz with the amplitude of 5 mV of LTP-F-2 after different cycles at a rate of 6 C.

4. CONCLUSION

Aqueous rechargeable lithium battery anode material $LiTi_2(PO_4)_3$/C was synthesized by using folic acid as a carbon source. High-quality carbon can improve electrical conductivity and protect the material structure. After the addition of folic acid, the electrochemical performance of composites was significantly improved with the following sequence: LTP < LTP-F-3 < LTP-F-1 < LTP-F-2. The discharge capacities of LTP-F-2 at 0.5, 4, and 15 C are determined to be 109, 108, and 95 mAh g^{-1},

respectively. LTP-F-2 exhibits excellent rate and cycling performances. The capacity after 1000 cycles at 6 C is measured to be 83 mAh g^{-1} with a capacity retention of 89.3%. Experimental results further demonstrate that high-quality carbon introduced from folic acid can greatly enhance the electrochemical performance of $LiTi_2(PO_4)_3$.

ACKNOWLEDGEMENTS
This research was funded by Henan Province Science and Technology Tackling Plan Project (No. 192102310233), State Key Laboratory of Advanced Technologies for Comprehensive Utilization of Platinum Metals (No. SKL-SPM-201923), and Major Special Projects in Henan Province (No. 201901AB0001).

References

1. I.Sowka, S. Pietrowicz, P. Kolasinski, *Energies*, 14 (2021) 1701.
2. C.X. Duan, Y. Yu, J. Xiao, Y.Y. Li, P.F. Yang, F. Hu, H.X. Xi, *Green Energy Environ.*, 6 (2021) 33.
3. H. Mikulcic, J. Baleta, X.B. Wang, N. Duic, R. Dewil, *J. Environ. Manage.*, 277 (2021) 111477.
4. L.J. Li, Z.Y. Chen, Q.B. Zhang, M. Xu, X. Zhou, H.L. Zhu, K.L. Zhang, *J. Mater. Chem. A*, 3 (2015) 894.
5. Y.K. Wang, G.Z. Zha, Y.N. Zhang, F. Liang, Y.N. Dai, Y.C. Yao, L.X. Kong, *Nano*, 16 (2021) 2150032.
6. H. Wang, Y. Yang, L. Guo, *Adv. Energy Mater.*, 7 (2017) 1601709.
7. Y.Q. Chu, H.X. Zhou, H.M. Zhao, *Int. J. Electrochem. Sci.*, 15 (2020) 7733.
8. Y.J. Ma, Y. Ma, H. Euchner, X. Liu, H. Zhang, B.S. Qin, D. Geiger, J. Biskupek, A. Carlsson, U. Kaiser, A. Gross, S. Indris, S. Passerini, D. Bresser, *ACS Energy Lett.*, 6 (2021) 915.
9. C. Liu, Z. Luo, W.T. Deng, W.F. Wei, L.B. Chen, A.Q. Pan, J.M. Ma, C.W. Wang, L.M. Zhu, L.L. Xie, X.Y. Cao, J.G. Hu, G.Q. Zou, H.S. Hou, X.B. Ji, *Acs Energy Lett.*, 6 (2021) 675.
10. R. Fang, W. Xiao, C. Miao, P. Mei, Y. Zhang, X.M. Yan, Y. Jiang, *Electrochim. Acta*, 317 (2019) 575.
11. H.H. Zhang, Z.G. Zou, S.C. Zhang, J. Liu, S.L. Zhong, *Int. J. Electrochem. Sci.*, 15 (2020) 12041.
12. Y. Huang, M.Y. Wang, Y.D. Zhu, X.S. Feng, L. Ding, Z.X. Guang, Y. Li, H.M. Zhang, N. Zhang, *Int. J. Energy Res.*, 44 (2020) 4910.
13. M.S. Zhao, B. Zhang, G.L. Huang, W.M. Dai, F. Wang, X.P. Song, *Energy Fuels*, 26 (2012) 1214.
14. D. Sun, Y.G. Tang, K.J. He, Y. Ren, S.Q. Liu, H.Y. Wang, *Sci. Rep.*, 5 (2015) 17452.
15. N. Alias, A.A. Mohamad, *J. Power Sources*, 274 (2015) 237.
16. W. Li, J.R. Dahn, D.S. Wainwright, *Science*, 264 (1994) 1115.
17. W. Tang, Y.S. Zhu, Y.Y. Hou, L.L. Liu, Y.P. Wu, K.P. Loh, H.P. Zhang, K. Zhu, *Energy Environ. Sci.*, 6 (2013) 2093.
18. Z. Jiang, Y.H. Li, J. Zhu, B. Li, C.C. Li, L. Wang, W. Meng, Z.X. He, L. Dai, *J. Alloy. Compd.*, 791 (2019) 176.
19. D. Sun, G.H. Jin, H.Y. Wang, P. Liu, Y. Ren, Y.F. Jiang, Y.G. Tang, X.B. Huang, *J. Mater. Chem. A*, 2 (2014) 12999.
20. N. Zhou, S.X. Huang, T. Hong, W. Luo, Y. Tian, X.Y. Lu, Z. Zhou, *Ceram. Int.*, 43 (2017) 9327.
21. Q.T. Qu, L.J. Fu, X.Y. Zhan, D. Samuelis, J. Maier, L. Li, S. Tian, Z.H. Li, Y.P. Wu, *Energy Environ. Sci.*, 4 (2011) 3985.
22. N. Liu, Z.X. He, X.B. Zhang, Y.Q. Jiang, Y.H. Li, J. Zhu, W. Meng, L. Dai, L. Wang, *Ceram. Int.*, 43 (2017) 11481.
23. M. Zhou, L. Liu, L.H. Yi, Z.H. Yang, S. Mao, Y.A. Zhou, T.T. Hu, Y. Yang, B.W. Shen, X.Y. Wang,

J. Power Sources, 234 (2013) 292.
24. V. Aravindan, W.C. Ling, S. Hartung, N. Bucher, S. Madhavi, *Chem. Asian J.*, 9 (2014) 878.
25. D. Sun, X. Xue, Y.G. Tang, Y. Jing, B. Huang, Y. Ren, Y. Yao, H.Y. Wang, G.Z. Cao, *ACS Appl. Mater. Interfaces*, 7 (2015) 28337.
26. C.B. Zhu, P. Kopold, W.H. Li, P.A. van Aken, J. Maier, Y. Yu, *Adv. Sci.*, 2 (2015) 1500200.
27. X.M. Li, S.J. Wang, X. Tang, R. Zang, P. Li, P.X. Li, Z.M. Man, C. Li, S.S. Liu, Y.H. Wu, G.X. Wang, *J. Colloid Interf. Sci.*, 539 (2019) 168.
28. Z.F. Huang, L. Liu, Q. Zhou, J.L. Tan, Z.C. Yan, D.D. Xia, H.B. Shu, X.K. Yang, X.Y. Wang, *J. Power Sources*, 294 (2015) 650.
29. Z. Zhou, A.H. Xiang, M. Xia, N. Zhou, *Ceram. Int.*, 44 (2018) 21599.
30. Z.X. He, Y.Q. Jiang, J. Zhu, H.Y. Wang, Y.H. Li, H.Z. Zhou, W. Meng, L. Dai, L. Wang, *Electrochim. Acta*, 279 (2018) 279.
31. J.Y. Luo, Y.Y. Xia, *Adv. Funct. Mater.*, 17 (2007) 3877.
32. Z.X. He, Y.Q. Jiang, W. Meng, J. Zhu, Y. Liu, L. Dai, L. Wang, *Electrochim. Acta*, 222 (2016) 1491.
33. G.M. Weng, L.Y.S. Tam, Y.C. Lu, *J. Mater. Chem. A*, 5 (2017) 11764.
34. Z.T. Liu, X.S. Qin, H. Xu, G.H. Chen, *J. Power Sources*, 293 (2015) 562.
35. J.X. Sun, Y.R. Sun, L.G. Gai, H.H. Jiang, Y. Tian, *Electrochim. Acta*, 200 (2016) 66.
36. J.M. Ye, C.M. Li, *Ionics*, 26 (2020) 2845.
37. M. Li, L. Liu, N. Zhang, S. Nie, Q.Y. Leng, J.J. Xie, Y. Ouyang, J. Xia, Y. Zhang, F.Y. Cheng, X.Y. Wang, *J. Alloy. Compd.*, 749 (2018) 1019